IEEE Access
Multidisciplinary | Rapid Review | Open Access Journal

Received 16 November 2023, accepted 3 December 2023, date of publication 7 December 2023,
date of current version 15 December 2023.

Digital Object Identifier 10.1109/ACCESS.2023.3340309

RESEARCH ARTICLE

GCN-Based Short-Circuit Current Calculation Method for Active Distribution Networks

RUIKAI YE, (Graduate Student Member, IEEE), HUIFANG WANG, (Member, IEEE), AND YIXIANG ZHANG
College of Electrical Engineering, Zhejiang University, Hangzhou 310027, China
Corresponding author: Huifang Wang (huifangwang@zju.edu.cn)

This work was supported in part by the Joint Funds of National Natural Science Foundation of China under Grant U2166204.

ABSTRACT The increasing integration of Inverter Interfaced Distributed Generators (IIDGs) into distribution networks has led to a more active nature of the grid. However, the accuracy-speed trade-off caused by iterative algorithms and simplified models in the short-circuit current calculation method for active distribution networks (ADNs) is becoming more prominent. To address this issue, we propose a novel approach that utilizes Graph Convolutional Neural Networks (GCNs) for short-circuit current calculation in ADNs. Our study explores the characteristics of short-circuit current in different network structures and evaluates the feasibility of representing electrical quantities using a graph data format. The proposed method employs the GCN model to calculate multi-output ADN short-circuit current and investigates the block construction of the GCN model. Algorithm analysis demonstrates that our method effectively calculates network-wide short-circuit current under various network structures, IIDG penetration rates, and fault conditions, meeting both accuracy and computational speed requirements. The proposed method offers several advantages, including superior precision, rapid computation, minimal hardware resource utilization, and robust resistance to interference.

INDEX TERMS Short-circuit current calculation, graph convolutional neural network, multi-output regression, inverter interfaced distributed generator, active distribution network.

I. INTRODUCTION

The global adoption of low-carbon targets has popularized the generation of new energy sources across the world. Integrating decentralized new energy into Active Distribution Networks (ADNs) enables the efficient development and utilization of Inverter Interfaced Distributed Generators (IIDGs), gradually transforming the distribution network into an active system [1].

The IIDGs introduce strong non-linear characteristics to the ADN, particularly affecting the short-circuit current after a fault incident [2]. This renders the conventional method for calculating short-circuit currents in distribution networks obsolete [3]. Short-circuit current calculations play a vital role in Relay Setting and Coordination, Fault Location, and Protection Equipment Selection. Consequently, many scholars have undertaken research in the field of ADN short-circuit current calculation, with the primary focus on enhancing calculation accuracy and speed [4], [5], [6], [7], [8].

In an effort to elucidate the alterations in ADN short-circuit current distribution following a fault occurrence, certain researchers have endeavored to formulate an intricate model for Inverter-Interfaced Distributed Generators (IIDGs) [7], [8], [9]. This detailed IIDG model comprehensively represents the transient-to-steady-state changes in current subsequent to an ADN fault [8]. While this detailed model exhibits a commendable ability to accurately compute ADN short-circuit current distribution, its complexity, and the intricate calculation procedures introduce unnecessary iterations, thereby diminishing calculation speed [9]. As the number of IIDGs in the system grows, the computational efficiency of the detailed model experiences a notable decline, and the potential for non-convergence becomes a concern in larger ADNs.

To enhance calculation speed, certain researchers have put forth a streamlined and refined approach for calculating

The associate editor coordinating the review of this manuscript and approving it for publication was Qiang Li.

short-circuit currents [10]. These simplification efforts can be categorized into two distinct approaches: one involves streamlining the iterative calculation procedures, while the other focuses on simplifying the IIDG model itself [11]. The streamlined iterative process can be further classified into two categories: enhancements to the iterative computation method and the disassembly of computational tasks based on the superposition theorem. Although the simplified iterative process yields more pronounced speed improvements, it comes with slightly stricter assumptions, potentially increasing the risk of inaccuracies in the short-circuit current calculations [12]. The simplified IIDG model primarily aims to linearize the post-fault output of IIDGs. This simplification often involves focusing solely on the output amplitude while disregarding the specific changes in active and reactive outputs, or it may exclusively consider the changes in reactive power while ignoring alterations in active power [13], [14]. Although these simplification methods for short-circuit current calculations effectively enhance calculation speed, they come at the cost of reduced accuracy or limited applicability due to the underlying assumption conditions [15].

Certain scholars have introduced a calculation approach founded on machine learning techniques to address the trade-off between speed and accuracy in current distribution calculations within ADNs [16], [17], [18]. The ML method tackles the accuracy issue in electric current calculations by learning the mapping between electrical characteristics and short-circuit currents. A substantial dataset of correspondences between ADN characteristics and short-circuit current distributions is gathered from comprehensive simulation models encompassing both ADN and IIDGs. ML methods demonstrate similar or smaller computational errors and faster computational speeds compared to detailed modeling methods. However, existing ML methods struggle to adapt to ADNs with different network structures, requiring retraining when the network structure changes. Developing a separate short-circuit current calculation model for each network structure is impractical, particularly in ADNs with numerous network structure combinations, which may lead to quantity disaster of the model.

The utilization of Graph Convolutional Neural Networks (GCN) and a graph data format for storing ADN information offers a promising solution as it preserves the network structure [19]. The GCN method exhibits robust capabilities for handling graph data while also retaining the inherent physical significance of the graph data itself [20].

Therefore, in this paper, we introduce a novel method based on GCN for calculating short-circuit currents in ADNs. Our approach addresses the trade-off between accuracy and speed that is typically encountered in traditional short-circuit current calculations, especially when there are changes in the network structure. The main objective is to train a short-circuit current calculation model capable of accurately determining the network-wide short-circuit current following any line fault in any network structure of the ADN. The contributions of this paper are as follows:

1) To concurrently achieve both accuracy and speed in ADN short-circuit current calculations, the GCN method is employed to address the challenge of necessitating multiple machine learning models due to topological shifts in network structure. Leveraging the sensitivity of GCN to graph topology and graph data, this approach can yield commendable model performance with a moderate quantity of samples, thereby enhancing the versatility of computational models.

2) By employing the line-graph concept, input features encompassing current characteristics, fault attributes, and IIDG features are amalgamated. The MP framework relays these input features along the shortest path within the network's topology, allowing the GCN method to discern various fault scenarios and IIDG outputs. This process enhances the precision of short-circuit current calculations.

3) Various ADNs with distinct network structures produce labeled current data that may exhibit a Long-Tail effect. The input features can be differentially distinguished by employing Laplacian matrix transformation, facilitating a distinctive mapping of the labeled current data and effectively mitigating the Long-Tail issue.

The structure of this article is as follows: In Section II, analyze IIDG's fault characteristic. In Section III, we delved into the GCN method and its application as a solution to the challenge of computing short-circuit currents in ADNs. Moving on to Section IV, we explored the approach centered around the GCN-based method for short-circuit current calculations, specifically focusing on addressing the Long-Tail challenge. Section V provides validation of the model through practical examples, encompassing scenarios encountered in real-world applications. Finally, in Section VI, we summarize the approach proposed in this paper.

II. FAULT ANALYSIS OF ADN

ADNs necessitate IIDGs to supply currents that align with the specific requirements contingent on the operational conditions. Consequently, IIDGs employ various control strategies, including voltage-controlled IIDGs (V/f-IIDG) and PQ-controlled IIDGs (PQ-IIDG). V/f-IIDG is predominantly employed in microgrids, while PQ-IIDG finds greater utility in ADNs that are interconnected with the primary grid [21].

In this paper, our focus is solely on ADNs that are interconnected with the primary grid. In such networks, the IIDGs produce only positive-sequence components in their outputs. When evaluating fault scenarios using a composite sequence network, the positive sequence network must account for the IIDG as an injected current source. In the event of a fault within the ADN, compliance with grid regulations mandates that IIDGs maintain a specified support voltage and refrain from disconnecting immediately. This requirement is known as Low Voltage Ride Through (LVRT) [22]. LVRT entails that IIDGs adjust their output current levels based on the voltage dips they experience. The specific equation governing LVRT

is as follows:

$$\begin{cases} I_q = 0 \\ I_d = \dfrac{S}{U_{PCC}} \end{cases} \quad U_{PCC} > 0.9U_N \tag{1a}$$

$$\begin{cases} I_q = K * I_N * (0.9 - \dfrac{S}{U_{PCC}}) \\ I_d = \sqrt{(K * I_N)^2 - I_q^2} \end{cases} \quad 0.2U_N \le U_{PCC} \le 0.9U_N \tag{1b}$$

$$\begin{cases} I_q = K * I_N \\ I_d = 0 \end{cases} \quad U_{PCC} < 0.2U_N \tag{1c}$$

where I_q and I_d are the reactive and active current components output from the IIDG, respectively. S is the IIDG capacity. U_{PCC} is the IIDG access bus voltage. U_N is the rated voltage, I_N is the rated current output from the IIDG, and K is the current limiting multiplier of the IIDG.

From (1), it highlights that the extent of voltage drop plays a pivotal role in determining the operating state of the IIDG. This determination hinges on variations in both reactive and active output levels. In (1b), an escalation in reactive output coincides with a reduction in active output, resulting in concurrent alterations in both the overall output magnitude and phase. This phenomenon represents a non-linear transformation process. Moreover, the output in (1b) assumes a complex form, introducing complexity into the calculation that involves complex numbers. In the context of short-circuit current calculations, this complexity poses challenges, increasing the computational difficulty, the number of iterations, and overall computation time.

The output formula is characterized by non-linearity, and the switching behavior of the three phases within the LVRT exhibits non-linear traits. These operation phases are continuous but lack differentiability concerning each other. When we can only ascertain that the IIDG is in one of the states (1a), (1b), or (1c), we can describe the IIDG's output using a computational formula. Furthermore, we can specify the output of the IIDG in this context. During the iterative calculation of short-circuit currents, each IIDG can exist in three possible output states, and when there are N IIDGs, the total number of potential output states for IIDGs following an ADN fault is 3^N. As the number of IIDGs increases, the complexity of ADN short-circuit current calculations surges, as evidenced by the exponential growth in the number of iterative computations, leading to a substantial increase in computational time.

Hence, the paramount challenge in conducting short-circuit current calculations for ADNs lies in precisely ascertaining the output of each IIDG following a fault event. Each specific fault scenario corresponds to a distinct set of IIDG output scenarios and distributions of steady-state short-circuit current [23]. Building upon this understanding, the GCN-based short-circuit current calculation method introduced in this paper demonstrates practical feasibility and applicability for ADNs.

III. GCN METHOD

A. GRAPH CONVOLUTIONAL NEURAL NETWORK AND MESSAGE PASSING

The graph is a form of unstructured data, represented using a set of nodes **V** and a set of connected edges **E**, i.e., the set of graphs is G = (V, E). The graph structure as shown in Fig. 1(a) has $\mathbf{V} = [v_1, \ldots, v_i, \ldots, v_6]$ denote the set of nodes, v_i are vectors containing N features; e_{ij} is the edge relationship between nodes v_i and v_j, and the set of e_{ij} is **E** [24].

GCN is an ML-based method that aggregates the feature information of nodes $\boldsymbol{V}$ based on connected edges $\boldsymbol{E}$ [25]. The aggregation process of graph data is shown schematically in Fig. 2. In the Fig. 2, v_{ab} denotes the $b-th$ node at $a-th$ layer, which is generated by aggregating node b at layer $a-1$ with its neighboring nodes. In Fig. 2, v_{32} in layer 3 can sense the feature information contained in the non-adjacent v_{14} nodes. This indicates that the GCN can effectively aggregate the feature information of the nodes on the graph.

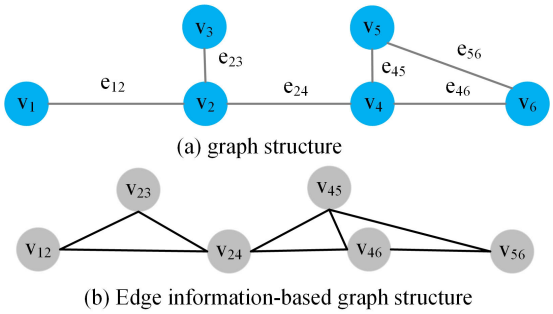

FIGURE 1. Example of graph structure.

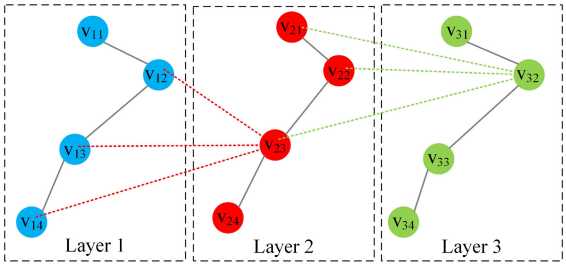

FIGURE 2. Schematic diagram of node aggregation of GCN.

In this paper, the MP method is chosen as the framework structure of the GCN method.MP can not only improve the aggregation ability of GCN, but also has the ability to improve the accuracy of the output [26]. The primary objective of the MP framework is to aggregate the information from multiple nodes while reducing the number of corresponding nodes. A full operation involving graph convolution and readout is referred to as a complete MP operation. The MP framework can be mathematically expressed as follows:

$$\tilde{X}, \tilde{A} = f_{softplus}(f_{readout}(f_{Conv}(\mathrm{X}, \mathrm{A}))) \tag{2}$$

where $\boldsymbol{X}$ denotes the input node feature for each MP operation, f_{Conv} denotes the convolution operation of MP, and $f_{readout}$ denotes the readout operation of readout, and each layer is processed using the activation function $f_{softplus}$ after the operation. Each layer of MP changes the node features and node connectivity relationships of the input graph. The new node features is $\tilde{\boldsymbol{X}}$ and the new adjacency matrix is $\tilde{\boldsymbol{A}}$.

$$\mathrm{Y}_{out} = f_{softplus}(W \cdot \tilde{X} + b) \tag{3}$$

The training process of MLP is essentially learning a weights matrix W and bias vectors b. The goal of MLP is to establish the mapping relationship between the final node $\tilde{\boldsymbol{X}}$ of MP and the output target $\boldsymbol{Y}_{out}$. The Softplus as an activation function is used to smooth the output values and prevent non-convergence. The final output target value is noted as $\boldsymbol{Y}_{out}$.

In ADN short-circuit current calculation, the near-fault short-circuit current is large, and the short-circuit currents of the upstream and downstream branches of the near IIDG buses will have IIDG boost or draw situations. The MP framework can increase or decrease the transmitted feature information according to the node distance of the graph data, which ensures that the near nodes feel more information and the far nodes feel less information. $\tilde{\boldsymbol{X}}$ in (3) has the property of conforming to the ADN short-circuit current distribution even though $\tilde{\boldsymbol{X}}$ converges to $\boldsymbol{Y}_{out}$. this reduces the possibility of the variation of W and b, which enhances the accuracy of the short-circuit current computation to some extent.

B. LAPLACIAN MATRIX

The graph data with different structures need to be processed for different structures in order to improve the GCN method's ability to perceive different network structures. The features corresponding to different structure graph can be extracted using the graph convolution Laplace matrix transform. The Laplace matrix transform needs to first express $\boldsymbol{E}$ as an adjacency matrix $\boldsymbol{A}$. Using $\boldsymbol{A}$, the degree of each node can be computed as $d(v_i)$. From $d(v_i)$, the degree matrix $\boldsymbol{D}$ can be formed, whose main diagonal element D_{ii} is expressed as:

$$D_{ii} = d(v_i) \tag{4}$$

The graph convolution Laplacian matrix $\boldsymbol{L}$ corresponding to the current $\boldsymbol{A}$ matrix is obtained using the adjacency matrix $\boldsymbol{A}$ and the degree matrix $\boldsymbol{D}$ [27]:

$$L = \boldsymbol{D} - \boldsymbol{A} \tag{5}$$

Using $\boldsymbol{L}$, the unit orthogonal feature vector ψ_+ can be found. Based on ψ_+, it can achieve different and unique projection mappings for graphs with different network structures. As a result, ψ_+ can achieve a unique vector transformation of the operation mode, fault conditions and IIDG outputs of ADNs with different network structures in the new orthogonal space. This can enable a GCN model to effectively handle the problem of short-circuit current calculation for ADNs with different structures. In addition, the use of Laplacian matrix to map the features to the new vector space for linearisation can improve the computational speed of the GCN model [28].Moreover, by using $\boldsymbol{L}$ and ψ_+, Kirchhoff's current law is still upheld when recreating the present operational state in the graph data of the ADN. Different network architectures can use this transformation [20].

C. ADN's GRAPH REPRESENTATION

For the graph representation, the ADN line should be treated as E and the ADN buses should be V. However, as mentioned earlier, the ADN operation is represented using the current values obtained from the line measurements. In order to be able to represent the current characteristics in a reasonable way, the graph representation in this paper chooses to use the line-graph approach for the representation [29]. It means that the branches of the original ADN as buses in the graph and the interconnected relationships between the branches as edges in the graph. In this regard, it needs to be treated as the representation of Fig. 1(b), where V_{ij} in Fig. 1(b) is represented as a node consisting of e_{ij} in Fig. 1(a).

The graph features of the ADN should include relevant information about the operational mode and faults in the normal state of the network. The normal operation of the ADN is characterized by the branch currents, which can be obtained through current measurements using current transformers installed at the first end of each branch. These branch currents provide valuable data for capturing the normal operating conditions of the ADN and are therefore incorporated as part of the graph features in the calculation process. The branch current information is three-phase current effective values $I_{A_i}, I_{B_i}, I_{C_i}$, where the subscript i indicates the i-th branch. The $I_{A_i}, I_{B_i}, I_{C_i}$ of all branches imply the operation of the distribution network. For two-phase or single-phase lines, the missing phase current is filled with 0. In addition to the branch current characteristics, the IIDG capacity value S_{DG_i} is also part of the operating mode. Fault information then contains fault type F_{type}, fault location F_{loc}, and fault transition resistance R_{on}. For a distribution network with K branches, each branch has the same number of graph node characteristics, and graph node v_i has the following characteristics:

$$v_i = \{I_{A_i}, I_{B_i}, I_{C_i}, S_{DG_i}, F_{\mathrm{type}}, F_{\mathrm{loc}}, R_{\mathrm{on}}\} \quad i = 1, 2, \cdots K \tag{6}$$

In (6), S_{DG_i} is unique to the IIDG branch and other branches are padded with zeros for this feature. F_{loc} indicates the percentage of the fault location from the head of the line, i.e. $F_{\mathrm{loc}} \subset [0, 1)$, and when $F_{\mathrm{loc}} = 0$, the fault is considered to have occurred at the head node. R_{on} is the transition resistance. F_{type} uses integers from 1 to 11 to indicate different types of faults. The F_{type}, F_{loc}, and R_{on} of non-faulted branches are filled with 0.

The ADN-specific graph node $\mathrm{V}_{\mathrm{ADN}}$ can be obtained using (6). Since the electrical characteristics of the ADN branches are chosen for the graph node characteristics, the edge set E is chosen for the connection relationship of the branches accordingly, which can construct the adjacency matrix $\mathrm{A}_{\mathrm{ADN}}$. The adjacency matrix $\mathrm{A}_{\mathrm{ADN}}$ can characterize

the present network structure of ADN. When the structure of ADN changes, the corresponding adjacency matrix A_{ADN} in the graph data also needs to be modified.

The graphs representing the ADN uniquely correspond to a set of network-wide short-circuit current distribution data, establishing a graph-wise mapping [30]. In the case of an ADN with K branches, the corresponding network-wide short-circuit current labeled values can be described as follows:

$$\boldsymbol{Y} = \left[y_{A_1}, y_{B_1}, y_{C_1}, \ldots, y_{A_i}, y_{B_i}, y_{C_i}, \ldots, y_{A_K}, y_{B_K}, y_{C_K}\right] \tag{7}$$

where $y_{A_i}, y_{B_i}, y_{C_i}$ are the A, B, and C three-phase short-circuit currents of the $i-th$ branch. For non-three-phase lines, tag value only has the phase which has current.

D. LOSS FUNCTION

The GCN needs to use the loss function after each training round to provide feedback to the network on the accuracy of the training. It is more appropriate to choose Mean Square Error (MSE) as the loss function, and for M outputs y has the following equation:

$$\mathrm{MSE} = \frac{\sum_{l=1}^{M} (y_{out}^{l} - y^{l})^2}{M} \quad l \in \{1, 2, \cdots, M\} \tag{8}$$

where y_{out}^{l} is the $l-$th predicted value of GCN and y^{l} is the $l-$th label value. When testing the training results with a test set after training is completed, the use of Mean Absolute Percentage Error (MAPE) as an evaluation metric can accurately measure the accuracy of the model regression predictions among widely varying target values. For M outputs y is the MAPE value calculated as follows:

$$\mathrm{MAPE} = \frac{100\%}{M} \times \sum_{l=1}^{M} \left| \frac{y_{out}^{l} - y^{l}}{y^{l}} \right| \tag{9}$$

The number of test sets is so large that it is difficult to show MAPE one by one. The mean $\mathrm{MAPE}_{\mathrm{mean}}$ of MAPE is used to indicate the average error of the model prediction, and its maximum $\mathrm{MAPE}_{\mathrm{max}}$ is used to indicate the error volatility.

IV. GCN-BASED SHORT-CIRCUIT CURRENT CALCULATION METHOD

A. GCN-BASED SHORT CIRCUIT CURRENT CALCULATION METHOD

The GCN method for calculating ADN short-circuit currents requires storing the ADN electrical information as a graph data structure. The graph data stores the ADN normal operation branch currents as node features according to (6), the connection relationships of the branches as $\tilde{\boldsymbol{A}}$ matrices, and the short-circuit current values of each branch as sample labels according to (7). Different ADN network structures are distinguished using the $\tilde{\boldsymbol{A}}$ matrix, and different ADN operation modes are distinguished using the (6) features. Any of the identified (6) features and the $\tilde{\boldsymbol{A}}$ matrix form a graph data sample that has a unique corresponding set of graph data labels as (7). A graph data sample and the corresponding set of labels constitute a single piece of graph data.

In the GCN method, the A matrix of each graph data is first decomposed using (5) to obtain ψ_+ that uniquely corresponds to different network structures. ψ_+ can map the information of nodes in the graph data to a new coordinate system. This can differentiate the features of different sample nodes of the same network structure, and also differentiate the features of nodes with similar values in different network structures.

Moreover, message passing is performed using (2) for the electrical information generated based on the network structure. The message passing mechanism passes the current information, IIDG information, and fault characteristics of each node to all nodes, so that each node can feel the effect of the current IIDG and fault characteristics on it. As the number of network layers for message passing increases, the value calculated for each node converges to its corresponding fault current. Finally the short-circuit current calculated at each node is output using (3).

The most important feature among the graph data of ADN is the $\tilde{\boldsymbol{A}}$ matrix of the current ADN. When the structure of ADN is changed, the corresponding $\tilde{\boldsymbol{A}}$ matrix needs to be modified first, and then the node features are obtained according to Eq. (6), and the output labels are obtained according to Eq. (7).

B. SHORT CIRCUIT CURRENT CALCULATION FLOW

The process of calculating the short-circuit currents in ADN using GCN can be divided into two main steps: obtaining data samples and training the GCN model. The detailed flowchart for the training process is illustrated in Fig. 3.

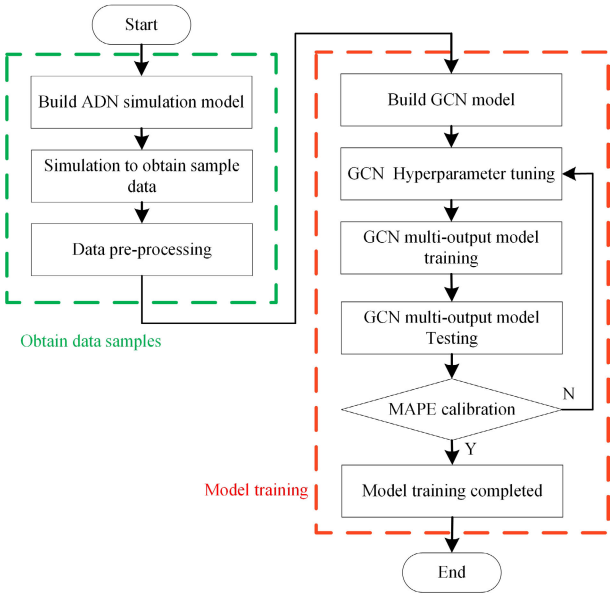

FIGURE 3. GCN Model training flow of short-circuit current calculation.

In the step of obtaining data samples, the initial stage involves constructing a comprehensive simulation model of

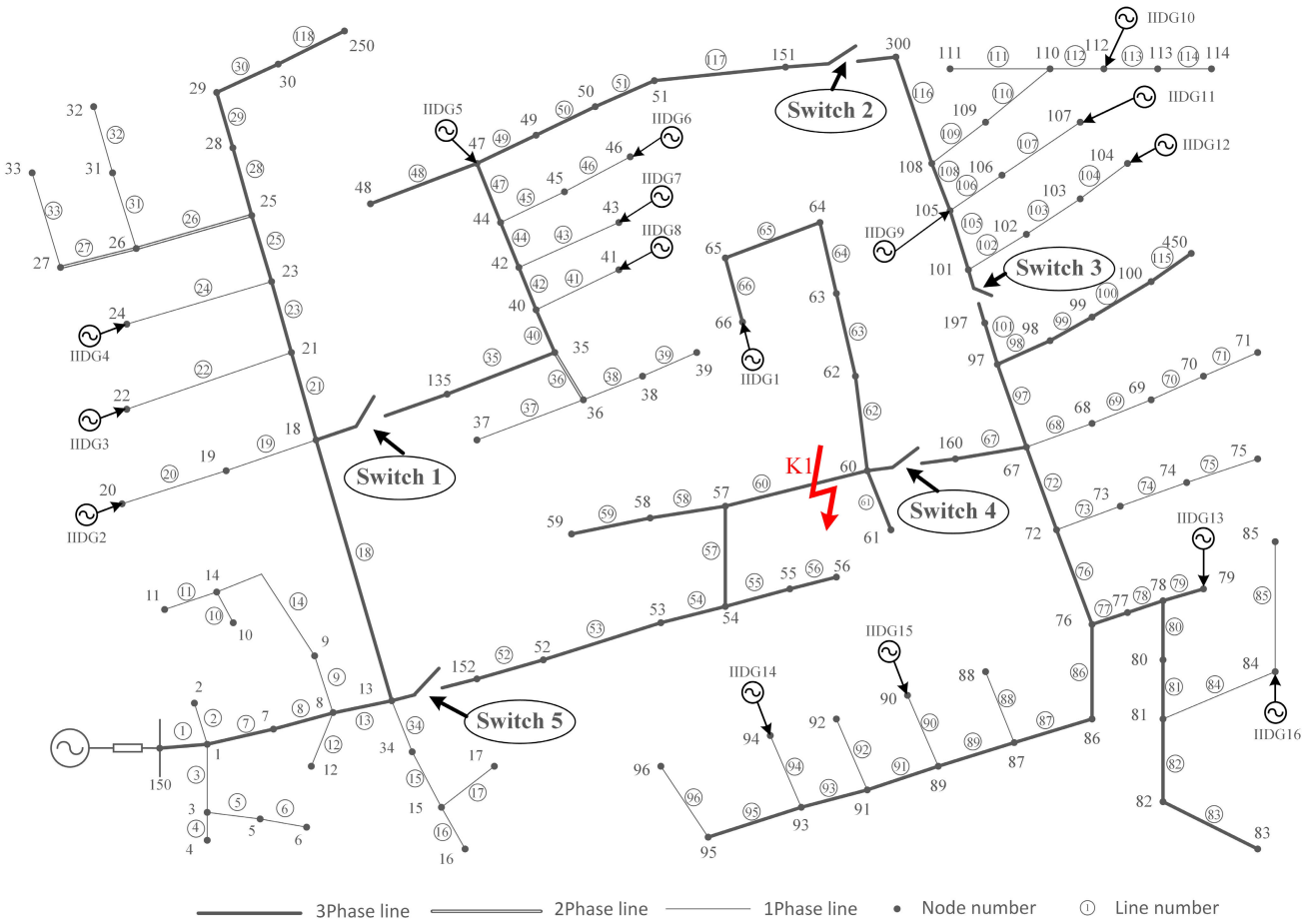

FIGURE 4. Structure of 123 node active distribution grid.

the ADN using Matlab/Simulink. The actual ADN is accurately modelled using matlab simulation software and the grid operation mode is obtained through simulation of accurate modelling. The fault conditions and locations are set in the accurate ADN model to obtain the corresponding short circuit current values. Subsequently, a significant volume of ADN sample data is acquired through simulation using the Matlab/Simulink model. The sample data is generated based on the criteria outlined in (6)-(7). Finally, the obtained sample data undergoes pre-processing procedures.

The features in V_{ADN} not only have a large range of values, but also have different physical meanings, so they need to be pre-processed. Numeric data needs to be normalized, and textual data needs to be given numeric identifiers. The pre-processed data are divided according to the network structure, with 80% of the data being the training set and the remaining 20% being the test set [31].

In the subsequent step of model training, the GCN model is constructed based on equations (2)-(3). The model is designed to accept pre-processed graph data as input, while the loss function employed is MSE. The objective of training the model is to acquire the optimal mapping relationship between the input and output. Upon satisfaction of the MSE conditions or completion of the specified number of training epochs, the model is evaluated using the test set and verified using MAPE. If the MAPE criterion is not met, adjustments to the hyperparameters of the GCN model are necessary. The aim of hyperparameter tuning is to minimize the MAPE.

The GCN-based short-circuit current calculation method can be trained offline and applied online. Using the actual ADN accurate modelling, the fault conditions and locations are set in the accurate ADN model to obtain the corresponding short-circuit current values. The training of the GCN short-circuit current calculation model is completed using the sample data obtained from the simulation. After the GCN model has been trained, it can be applied to the ADN online. When applied online, the short-circuit current value calculated by the GCN model can be used as the reference value of fault current, which is of some significance for the online adjustment of relay protection. The short-circuit currents calculated using the GCN model can also be applied to quickly locate the location of the fault occurrence in order to reduce the workload of the field staff.

C. CHALLENGE OF CHANGING NETWORK STRUCTURE

The short-circuit current distributions in ADNs can vary depending on the network structure, even under the same fault conditions. Additionally, the short-circuit current values of individual branches can exhibit significant variations due to differences in network structures. To illustrate this point, we consider the IEEE 123 nodes ADN depicted in Fig. 4, which consists of 5 switches. During normal operation, only one switch is open while the rest remain closed to ensure acyclic operation. Consequently, there are five distinct network structures [32]. In the event of a fault occurring at position K1, the magnitude of the short-circuit current measured at the branch connecting branch 54-57 is directly influenced by the specific network structure in place.

When any of switch1, switch2, switch3, or switch4 is activated, the short-circuit current from the system power supply directly passes through branch 54-57, resulting in a significantly high measured short-circuit current exceeding 100A. However, when switch5 is activated, neither the system power supply nor the IIDG provides any short-circuit current to branch 54-57. As a result, the measured current value is very low, less than 1A. This observation highlights the substantial variation in short-circuit current values across branch 54-57, with differences exceeding thousands of times or more. This situation where a small number of samples have a large impact is called Long-Tail [33].

By utilizing GCN and ψ_+, it is possible to overcome the Long-Tail issue which cause conflict between balancing network structure samples and balancing target values. Different ψ_+ can realize the projection of graph data of different network structures on different bases, which can effectively distinguish the input features of different network structures. This can solve in principle the difficult problem of changing target prediction due to changes in network structure.

However, during the process of deep learning, the computation of the graph convolution Laplacian matrix is susceptible to the issues of gradient explosion or gradient disappearance. To address this challenge, [34] proposed the concept of renormalization in GCN networks in. This innovative approach mitigates the problems associated with gradient instability. Consequently, in this paper, the GCN method incorporating the concept of renormalization is selected as the model for calculating short-circuit currents.

V. ALGORITHM VALIDATION

A. CASE STUDY

To assess the efficacy of the GCN-based ADN short-circuit current calculation method, the IEEE 123 node system is employed as an illustrative case study. This system, along with the corresponding IIDG connection locations, is depicted in Fig. 4. The system power connection point is denoted by node 150, with an ADN voltage level of 4.16kV. The total load in the system is 3557kW, and the penetration rate of IIDG is approximately 50%.

To simulate the actual system operation, IIDG capacity and load size were randomly generated within [0.8, 1.2] times of their original values. The original values are from [32]. IIDG adopts a network-following type of control strategy. IIDG capacities from IIDG1 to IIDG16 are 300kw, 20kw, 20kw, 20kw, 300kw, 10kw, 10kw, 10kw, 10kw, 300kw, 20kw, 20kw, 20kw, 20kw, 400kw, 20kw, 20kw, 20kw respectively. The random fluctuations of the parameters cover the cases of IIDG penetration rates in [20%, 80%]. The penetration rates are obtained in groups of 1% each, for a total of 60 different sets of penetration rate cases, which is the same grouping method as in [30]. When setting the fault, F_{line} is randomly selected and the fault types F_{type}, F_{loc} and R_{on} are randomly set according to F_{line} The F_{loc} setting range is 20% of the line length as a group and five fault line ranges are selected. R_{on} range is [1, 1000] and five transition resistance cases are randomly selected. the setting range of transition resistance should match the fault type. For the way the fault conditions are set refer to [35].

For each line, a total of 25 fault combinations are generated, resulting in 25 different fault conditions. In the case of the IEEE 123 node ADN, five distinct network structures are created by sequentially disconnecting five contact switches. The network structure is represented by the adjacency matrix in the graph data. To cover all fault scenarios on each line under each network structure, a total of 1500 sets of data are required. Since three-phase short circuits are considered the most severe faults in ADN, the calculation example focuses on three-phase faults. Other fault types are handled similarly to three-phase short circuits. Therefore, this paper requires 495,000 sets of data, encompassing 66 three-phase branched short circuits under five network structures. The GCN model uses sample data from the 123-node model simulation of Figure 4. The network in Fig.4 is from [32], and the description of the parametric model in this section is a modified description of [32]. All other ADN networks can be used in this way for sample simulation and training using the GCN model in this paper.

B. GCN MODEL TRAINING

In (2)-(3), the specific number of MP layers and MLP layers cannot be determined directly. The optimal number of layers needs to be determined through experimentation. The experiments conducted on the GCN network layers are summarized in Table 1. In the MP layers, the number of output nodes is set to 256. The notation ''1-layer MP'' indicates the use of a single MP layer with 256 convolutional kernels. Similarly, ''2-layer MP'' refers to the use of two MP layers with 128 and 256 convolutional kernels respectively. For ''3-layer MP,'' three MP layers are employed with 64, 128, and 256 convolutional kernels respectively.

Through the experiment, it can be seen that when the number of messaging layers is determined, the influence of the number of MLPs on the final output $\text{MAPE}_{\text{mean}}$ is more obvious, and regardless of the number of messaging layers, MLPs

TABLE 1. Experimental results of gcn model structure.

Structure of GCN		Performance	
Num of MP	Num of MLP	$MAPE_{mean}$ (%)	$MAPE_{max}$ (%)
1	1	0.104	0.543
	2	0.034	0.699
	3	0.041	0.755
	4	0.034	0.757
2	1	0.104	0.458
	2	0.037	0.594
	3	0.038	0.662
	4	0.040	0.661
3	1	0.103	0.507
	2	0.041	0.700
	3	0.043	0.648
	4	0.036	0.728

choose 2 layers to have the optimal $MAPE_{mean}$. While the number of layers of MP is more correlated with $MAPE_{max}$, the same MLP layers have smaller $MAPE_{max}$ when MP is 2 layers, which means that the output target value has higher overall accuracy with less volatility. Therefore, the structure of the GCN model is determined as 2-layer MP with 2-layer MLP. The model structure is same as (2)-(3) while the epochs are set to 500 and batch size is 64 for hyperparameters tuning of the model. The learning rate is variable, with $10e^{-4}$ for the first 150 epochs, $10e^{-5}$ for 150-350 epochs, and $10e^{-6}$ for the last 150 epochs. The multi-output model training platform uses a CPU of the i7-9900K and version 3.8.8 of Python.

C. MODEL PERFORMANCE COMPARISONS

The effectiveness of ML-based multi-output methods for short-circuit currents has been previously demonstrated in the literature [18]. In this paper, two representative methods, namely Multi-Target Regressor Stackin-LightGBM (MTRS-LightGBM) and Regression Chain - LightGBM (RC-LightGBM), from the problem transformation approach, are selected for comparison with the GCN multi-output methods. To validate the effectiveness of the ML method, the computational performance of the traditional iterative method is used for cross-comparison validation. The Newton Raphson method is chosen for the conventional iterative method. Also, a comparison is made with the short circuit current calculation method using simplified model. The simplified model for IIDG uses a simplification method that considers IIDG as (1c) only. This is a simplified method where the IIDG fully outputs reactive current.

The datasets used in the comparison are obtained from the simulation of the IEEE 123 ADN, specifically from the network structure where the contact switch at branch 57-60 is disconnected (as shown in Fig. 4). The GCN method utilizes graph-based data storage, while the datasets for MTRS-LightGBM and RC-LightGBM employ a structured data storage format. Since the network structure is fixed, a total of 99,000 data sets are used, with 79,200 sets allocated for training and 19,800 sets for testing. The comparison results are presented in Table 2, where the better performing method for each metric is highlighted in bold font. The "test time" in Table 2 refers to the duration required to process the test dataset.

TABLE 2. Performance comparison of different methods.

Multi-output model	$MAPE_{mean}$ (%)	$MAPE_{max}$ (%)	Train time (s)	Test time (s)	Model size (MB)
MTRS-LightGBM	**0.005**	**0.021**	1098.120	19.587	175.045
RC- LightGBM	0.050	0.240	5031.576	9.048	191.757
GCN	0.015	0.382	**1927.994**	**2.307**	**1.07**
Newton	0.060	0.202	/	3785.61	/
Simplified Model	0.106	1.149	/	96.58	/

The results in Table 2 demonstrate that the GCN-based short-circuit current multi-output regression, within the fixed network structure, achieves results closer to the true values compared to the problem transformation method. The GCN approach not only enhances the calculation speed but also ensures accuracy, thereby addressing the trade-off between accuracy and speed in ADN short-circuit current calculations. Additionally, the GCN model has a smaller size, resulting in reduced storage requirements and hardware footprint.

Compared with the iterative method, the GCN method has a lower overall average error, and it can be considered that the GCN method has a similar accuracy to the traditional Newton iterative method. And the GCN method can substantially improve the speed of short-circuit current calculation. Compared to the method using simplified model, the GCN method has better performance in terms of both speed and accuracy. Although the speed of the simplified model method is close to that of the GCN method, its accuracy fluctuates greatly. In particular, currents in branches far from the fault location and with nearby IIDGs are prone to large deviations in accuracy.

The performance comparison between the GCN algorithm, MTRS-LightGBM, and RC-LightGBM was conducted using data from different network structures, and the results are presented in Table 3 and Fig. 5. Table 3 provides an overview of the performance comparison among the three methods using data from five network structures. On the other hand, Fig. 5 illustrates the performance variation of the three methods as the number of structures increases from 1 to 5.

According to Table 3, the GCN method exhibits superior performance compared to traditional ML methods across five different network structures. In contrast to Table 2, where the network structure was fixed, MTRS-LightGBM and RC-LightGBM methods experience a more than tenfold decrease in accuracy under the five network structures, while the GCN method demonstrates minimal changes in accuracy. The error fluctuations, represented by $MAPE_{max}$, are significantly higher for the problem transformation methods,

TABLE 3. Performance comparison of multiple output models with network structure change.

Multi-output model	$Mape_{mean}$ (%)	$MAPE_{max}$ (%)
MTRS-LightGBM	0.255	14.256
RC- LightGBM	0.190	10.883
GCN	**0.037**	**0.594**

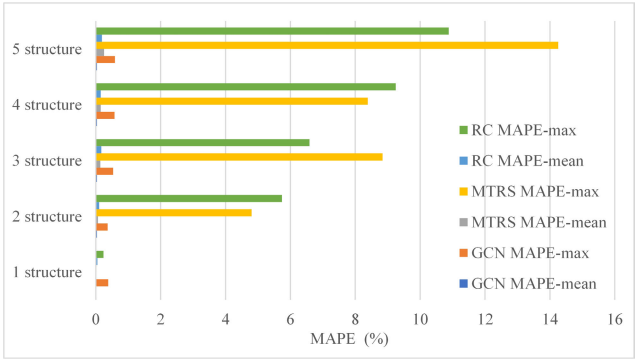

FIGURE 5. Performance of different models with different network structures.

reaching up to 14.256%. Such fluctuations of 14% indicate the inadequacy of the traditional ML methods in handling multiple outputs of ADN short-circuit current with varying network structures. In contrast, the GCN method exhibits error fluctuations below 0.6%, which is within an acceptable range. This implies that the GCN method is capable of meeting the requirements for short-circuit current calculation in ADNs with diverse network structures. Fig. 5 further illustrates the performance variations of different multi-output methods as the number of network structures increases. The error volatility of MTRS-LightGBM and RC-LightGBM methods significantly grows, while the error fluctuations of the GCN remain relatively smooth.

D. ANTI-INTERFERENCE CAPABILITY OF MODELS

In real-world applications, it is common to encounter data loss during data acquisition and transmission. To compensate for this lost data, a random zeroing technique is applied to the input features of the test set, where each random loss represents the loss of three-phase data for a specific node. The 123 nodes in Figure 4 have a total of 118 lines, and there are 118 nodes in the GCN. Data loss is handled by randomly setting all current data to zero at any number of nodes in each graph data. When X branch currents are lost, there is loss rate =X/118.

The control group continues to use the problem transformation method, and its performance under different data loss ratios is presented in Table 4 and Fig. 6. In Table 4, the values highlighted in bold indicate smaller error data, reflecting better performance. Columns 3 to 5 of Table 4 represent model training and testing using data from determined network structures, while the last column indicates the interference resistance of the models trained with data from the five network structures.

TABLE 4. Performance comparison of multi-output model with different rates of data loss.

Percentage of Data Loss	Performance	MTRS LightGBM	RC LightGBM	GCN Single network	GCN Different network
1%	$MAPE_{max}$ (%)	**0.265**	1.097	0.321	0.659
	$MAPE_{mean}$ (%)	0.051	0.099	**0.016**	0.037
3%	$MAPE_{max}$ (%)	0.508	2.264	**0.470**	0.797
	$MAPE_{mean}$ (%)	0.106	0.207	**0.018**	0.060
5%	$MAPE_{max}$ (%)	0.774	4.552	**0.502**	1.280
	$MAPE_{mean}$ (%)	0.145	0.302	**0.024**	0.077
10%	$MAPE_{max}$ (%)	2.211	6.532	**1.342**	1.907
	$MAPE_{mean}$ (%)	0.292	0.545	**0.104**	0.145

From Table 4, it can be observed that when the data loss is below 3%, the performance of MTRS-LightGBM and GCN methods is comparable. However, the GCN method exhibits higher accuracy, although its output fluctuation is slightly larger compared to MTRS-LightGBM. As the amount of data loss exceeds 5%, the advantage of GCN becomes more pronounced, with improved accuracy and reduced output fluctuation. When the data loss is below 10%, the GCN method demonstrates higher resistance to interference and shows minimal fluctuations due to network structure changes and data loss, ensuring higher availability compared to the problem transformation methods.

Fig. 6 depicts a performance comparison between the GCN method and the problem transformation method for a high percentage of lost data. It provides a visual representation of the accuracy and fluctuation of the output for both methods under different levels of data loss. The graph highlights the performance of the GCN method with bold values, indicating smaller error data. The $MAPE_{mean}$ of each method is low. However, the $MAPE_{max}$ grows rapidly after the amount of data loss reaches 20%, which means that the regressed short-circuit current values fluctuate widely and some branch currents have exceeded the acceptable range. However, the GCN is an order of magnitude smaller than the problem transformation method in terms of $MAPE_{max}$, and when GCN is lost by 50%, the $MAPE_{max}$ is similar to that of the problem transformation method when the data is lost by 40%.

Consequently, the GCN method exhibits superior anti-interference ability, successfully regressing the overall fluctuation of short-circuit current values even within a 20% data loss scenario. This remarkable resilience of GCN is crucial for its practical engineering application since significant deviations in accuracy only occur when the data loss rate exceeds 20%. Thus, the GCN method proves to be highly reliable and suitable for real-world deployment in scenarios with potential data loss.

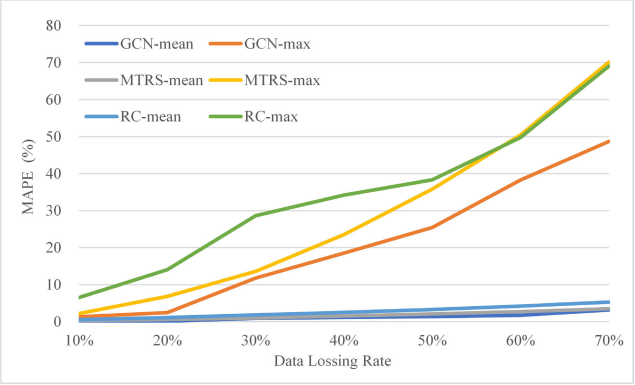

FIGURE 6. MAPE comparison for different methods under high proportion of data losing.

VI. CONCLUSION

IIDG's output during a short-circuit fault in an ADN exhibits strong non-linear behavior. This strong non-linear behavior affects both the calculation accuracy and computational speed of the iterative method employed to determine the short-circuit current.

The non-linear behavior of IIDG's output during a short-circuit fault in an ADN has a significant impact on both the accuracy and computational speed of the iterative method used to determine the short-circuit current. When there is a large quantity of IIDGs and the network size is substantial, the aforementioned paradox becomes even more pronounced. Although ML combined with structured data input does not inherently compromise computational accuracy and speed, its ability to handle diverse network structures is limited. To address this limitation, this study presents a novel multi-output model for short-circuit current estimation based on GCN. This model effectively incorporates both the network structure and real-world electrical measurements, offering a viable solution to the challenge of accurately calculating short-circuit current. Notably, the proposed model can be seamlessly adapted to different structured ADNs using a single model. In conclusion, it can be inferred that:

1) The GCN multi-output model demonstrates remarkable efficiency and accuracy in predicting network-wide short-circuit currents, particularly when encountering different branch faults under a predetermined network structure. Additionally, its compact size results in substantial savings in hardware resource usage and computational time during real-time applications.

2)The GCN approach exhibits a remarkable sensitivity to the adjacency of network structures, enabling it to precisely capture the mapping relationship across diverse network configurations. This capability addresses the challenge of handling separate network architectures that may lead to significantly varying target values, thereby enhancing the accuracy of regression tasks. As a result, the proposed approach holds great practical relevance.

3) The GCN multi-output model showcases strong resilience to interference, particularly when dealing with sampled data loss within the actual grid. Even under conditions where the data loss ratio reaches up to 20%, the model remains operational and continues to provide reliable predictions for short-circuit currents, ensuring robust performance in real-world scenarios.

The GCN-based short-circuit current calculation method still has some limitations. The more network structure of AND changes, the larger the error of short-circuit current obtained from the regression of GCN model. When the ADN network structure changes significantly, it is suggested that the GCN model needs to be retrained. The GCNs retrained based on ADNs of different network structures are all applicable to the current network structure used for GCN training. And the GCN model converges regardless of the current number of ADN nodes. In future research, the impact of network structure changes on the output accuracy of the GCN model can be further reduced by reconfiguring the graph data node features or adjusting the GCN perception method of the graph data.

REFERENCES

[1] C. A. Plet, M. Brucoli, J. D. F. McDonald, and T. C. Green, "Fault models of inverter-interfaced distributed generators: Experimental verification and application to fault analysis," in *Proc. IEEE Power Energy Soc. Gen. Meeting*, Jul. 2011, pp. 1–8.

[2] K. H. M. Azmi, N. A. M. Radzi, N. A. Azhar, F. S. Samidi, I. T. Zulkifli, and A. M. Zainal, "Active electric distribution network: Applications, challenges, and opportunities," *IEEE Access*, vol. 10, pp. 134655–134689, 2022.

[3] H. Shin, J. Jung, and B. Lee, "Determining the capacity limit of inverter-based distributed generators in high-generation areas considering transient and frequency stability," *IEEE Access*, vol. 8, pp. 34071–34079, 2020.

[4] W.-M. Guo, L.-H. Mu, and X. Zhang, "Fault models of inverter-interfaced distributed generators within a low-voltage microgrid," *IEEE Trans. Power Del.*, vol. 32, no. 1, pp. 453–461, Feb. 2017.

[5] L. Wieserman and T. E. McDermott, "Fault current and overvoltage calculations for inverter-based generation using symmetrical components," in *Proc. IEEE Energy Convers. Congr. Expo. (ECCE)*, Sep. 2014, pp. 2619–2624.

[6] X. Wang, X. Sheng, W. Qiu, W. He, J. Xu, Y. Xin, and J. Jv, "Fault reconfiguration strategies of active distribution network with uncertain factors for maximum supply capacity enhancement," *IEEE Access*, vol. 10, pp. 72373–72380, 2022.

[7] S. Yuan, B.-F. Yang, and J.-Y. Zhang, "Experimental study on short-circuit current characteristics of a photovoltaic system with low voltage ride through capability under a symmetrical fault," *Energy Rep.*, vol. 8, pp. 4502–4511, Nov. 2022.

[8] S. Chiniforoosh, J. Jatskevich, A. Yazdani, V. Sood, V. Dinavahi, J. A. Martinez, and A. Ramirez, "Definitions and applications of dynamic average models for analysis of power systems," *IEEE Trans. Power Del.*, vol. 25, no. 4, pp. 2655–2669, Oct. 2010.

[9] S. P. Pokharel, S. M. Brahma, and S. J. Ranade, "Modeling and simulation of three phase inverter for fault study of microgrids," in *Proc. North Amer. Power Symp. (NAPS)*, Sep. 2012, pp. 1–6.

[10] Q. Wang, N. Zhou, and L. Ye, "Fault analysis for distribution networks with current-controlled three-phase inverter-interfaced distributed generators," *IEEE Trans. Power Del.*, vol. 30, no. 3, pp. 1532–1542, Jun. 2015.

[11] Z. Shuai, C. Shen, X. Yin, X. Liu, and Z. J. Shen, "Fault analysis of inverter-interfaced distributed generators with different control schemes," *IEEE Trans. Power Del.*, vol. 33, no. 3, pp. 1223–1235, Jun. 2018.

[12] L. Strezoski, M. Prica, and K. A. Loparo, "Generalized Δ-circuit concept for integration of distributed generators in online short-circuit calculations," *IEEE Trans. Power Syst.*, vol. 32, no. 4, pp. 3237–3245, Jul. 2017.

[13] J. Yin, "An improved fault current calculation method and protection scheme of doubly-fed induction generator," *Energy Rep.*, vol. 7, pp. 5168–5174, Nov. 2021.

[14] R. Zamani, M. E. H. Golshan, H. H. Alhelou, and N. Hatziargyriou, "A novel synchronous DGs islanding detection method based on online dynamic features extraction," *Electr. Power Syst. Res.*, vol. 195, Jun. 2021, Art. no. 107180.
[15] S. D. Jin, Y. Q. Song, C. J. Fan, S. Jiang, and X. Li, "Calculation of current protection setting based on inverter generation control strategy," *Power Syst. Technol.*, vol. 45, no. 9, pp. 3690–3699. Dec. 2021.
[16] C. Zhang, K. Peng, H. Li, B. Xu, and Y. Chen, "Fault calculation method of distribution network based on deep learning," *Symmetry*, vol. 13, no. 6, p. 1086, Jun. 2021.
[17] X. Zheng, H. Wang, K. Jiang, and B. He, "A novel machine learning-based short-circuit current prediction method for active distribution networks," *Energies*, vol. 12, no. 19, p. 3793, Oct. 2019.
[18] R. K. Ye, H. F. Wang, S. Zhang, and Y. X. Zhang, "Data-driven multi-output model for short-circuit current calculation in distribution network with IIDGs," *Electr. Power Autom. Equip.*, vol. 42, no. 9, pp. 1–8. Dec. 2022.
[19] Y. Zhai, Q. Wang, X. Yang, Z. Zhao, and W. Zhao, "Multi-fitting detection on transmission line based on cascade reasoning graph network," *IEEE Trans. Power Del.*, vol. 37, no. 6, pp. 4858–4868, Dec. 2022.
[20] Y. H. Wang, J. Shen, Q. Zeng, Y. T. Fu, and W. Ye, "Voltage estimation for DC grid nodes based on spectral theory and graph convolutional neural network," *Power Syst. Technol.*, vol. 46, no. 2, pp. 521–532. Apr. 2022.
[21] Q. Liu, K. Jia, B. Yang, L. Zheng, and T. Bi, "Analytical model of inverter-interfaced renewable energy sources for power system protection," *IEEE Trans. Power Del.*, vol. 38, no. 2, pp. 1064–1073, Apr. 2023.
[22] J. Song, M. Cheah-Mane, E. Prieto-Araujo, and O. Gomis-Bellmunt, "Short-circuit analysis of grid-connected PV power plants considering inverter limits," *Int. J. Electr. Power Energy Syst.*, vol. 149, Jul. 2023, Art. no. 109045.
[23] J. Song, M. Cheah-Mane, E. Prieto-Araujo, and O. Gomis-Bellmunt, "Short-circuit analysis of AC distribution systems dominated by voltage source converters considering converter limitations," *IEEE Trans. Smart Grid*, vol. 13, no. 5, pp. 3867–3878, Sep. 2022.
[24] Z. Wang, M. Xia, M. Lu, L. Pan, and J. Liu, "Parameter identification in power transmission systems based on graph convolution network," *IEEE Trans. Power Del.*, vol. 37, no. 4, pp. 3155–3163, Aug. 2022.
[25] Y. Wang, J. Yan, Z. Yang, Z. Qi, J. Wang, and Y. Geng, "A novel domain adversarial graph convolutional network for insulation defect diagnosis in gas-insulated substations," *IEEE Trans. Power Del.*, vol. 38, no. 1, pp. 442–452, Feb. 2023.
[26] I. Spinelli, S. Scardapane, and A. Uncini, "Adaptive propagation graph convolutional network," *IEEE Trans. Neural Netw. Learn. Syst.*, vol. 32, no. 10, pp. 4755–4760, Oct. 2021.
[27] R. Ying, R. He, K. Chen, P. Eksombatchai, W. L. Hamilton, and J. Leskovec, "Graph convolutional neural networks for web-scale recommender systems," in *Proc. 24th ACM SIGKDD Int. Conf. Knowl. Discovery Data Mining*, Jul. 2018, pp. 974–983.
[28] M. Khodayar and J. Wang, "Spatio-temporal graph deep neural network for short-term wind speed forecasting," *IEEE Trans. Sustain. Energy*, vol. 10, no. 2, pp. 670–681, Apr. 2019.
[29] G. Duan, H. Lv, H. Wang, and G. Feng, "Application of a dynamic line graph neural network for intrusion detection with semisupervised learning," *IEEE Trans. Inf. Forensics Security*, vol. 18, pp. 699–714, 2023.
[30] C. Li, Z. Dong, G. Chen, B. Zhou, J. Zhang, and X. Yu, "Data-driven planning of electric vehicle charging infrastructure: A case study of Sydney, Australia," *IEEE Trans. Smart Grid*, vol. 12, no. 4, pp. 3289–3304, Jul. 2021.
[31] L. Cheng, H. Zang, T. Ding, Z. Wei, and G. Sun, "Multi-meteorological-factor-based graph modeling for photovoltaic power forecasting," *IEEE Trans. Sustain. Energy*, vol. 12, no. 3, pp. 1593–1603, Jul. 2021.
[32] *IEEE PES Distribution Systems Analysis Subcommittee Radial Test Feeders*. Accessed: May 2017. [Online]. Available: http://www.ewh.ieee.org/soc/pes/dsacom/testfeeders/index.html
[33] Z. Sun, W. Hu, C. Wang, Y. Wang, and Y. Qu, "Revisiting embedding-based entity alignment: A robust and adaptive method," *IEEE Trans. Knowl. Data Eng.*, vol. 35, no. 8, pp. 8461–8475, Aug. 2023.
[34] T. N. Kipf and M. Welling, "Semi-supervised classification with graph convolutional networks," 2017, *arXiv.1609.02907*.
[35] X. Weihong, M. Xinghua, and L. Jinglua, "Influence of small resistance grounding mode on personal safety and research of intelligent resistance grounding mode," *Power Syst. Protection Control*, vol. 47, no. 14, pp. 166–172, Sep. 2019.

RUIKAI YE (Graduate Student Member, IEEE) received the M.Sc. degree from the Sichuan University of Science and Engineering, Zigong, China, in 2019. He is currently pursuing the Ph.D. degree in electrical engineering with Zhejiang University, Hangzhou, China. His research interests include the application of machine learning in power systems, adaptive protection, and short-circuit current calculation of active distribution systems.

HUIFANG WANG (Member, IEEE) received the B.Sc. and M.Sc. degrees from North China Electric Power University, Baoding, China, in 1995 and 1998, respectively, and the Ph.D. degree from Zhejiang University, Hangzhou, China, in 2006. Currently, she is an Associate Professor with the Electrical Engineering College, Zhejiang University. Her research interests include the application of artificial intelligence techniques in power systems, power system protection, and condition based maintenance.

YIXIANG ZHANG received the B.Sc. degree from Zhejiang University, Hangzhou, China, in 2021, where he is currently pursuing the Ph.D. degree in electrical engineering. His research interest includes the application of artificial intelligence techniques in power systems.